ISSN 1029-9599, Physical Mesomechanics, 2019, Vol. 22, No. 1, pp. 65–72. © Pleiades Publishing, Ltd., 2019.
Russian Text © I.G. Goryacheva, F.I. Stepanov, E.V. Torskaya, 2018, published in Fizicheskaya Mezomekhanika, 2018, Vol. 21, No. 6, pp. 66–74.

Fatigue Wear Modeling of Elastomers

I. G. Goryacheva, F. I. Stepanov, and E. V. Torskaya*

Ishlinsky Institute for Problems in Mechanics, Russian Academy of Sciences, Moscow, 119526 Russia
** e-mail: torskaya@mail.ru*

Received November 15, 2018, revised November 15, 2018, accepted November 22, 2018

Abstract—This study presents modeling results on fatigue wear of elastomers. A contact problem solution has been derived for the sliding of a system of asperities over a viscoelastic half-space. The mechanical properties of the viscoelastic half-space are described by relations between stresses and strains given by the Volterra integral operator. The contact problem is solved by the boundary element method using an iterative procedure. Stresses in the subsurface layers of the viscoelastic material are analyzed. The damage function of the surface layer is calculated using a reduced stress criterion, the parameters of which are determined on the basis of available experimental data. The wear process is studied under the assumption that the accumulated damage can be summed up. Within the applied frictional interaction model, the wear process presents the delamination of material surface layers of finite thickness at discrete points in time and continuous surface wear by fatigue mechanism. A model calculation of contact fatigue damage accumulation has shown that the time to the first material delamination (incubation period) depends on the sliding velocity and the viscoelastic properties of the material. By analyzing the dependence of the wear rate on the input parameters of the problem, it was investigated how the sliding velocity affects the time of fatigue damage initiation and the run-in and steady-state wear rates in materials with different rheological properties. Model calculations revealed that the wear rate of material surface layers after the incubation period increases smoothly and then stabilizes. The presence of the steady-state wear rate agrees well with experimental data. The developed method for studying fatigue damage accumulation in the surface layers of viscoelastic materials in frictional interaction can also be applied on the macrolevel to determine possible crack initiation sites.

DOI: 10.1134/S1029959919010107

Keywords: contact fatigue, damage accumulation, wear, viscoelasticity

1. INTRODUCTION

Modeling and experimental study of wear of elastomers is an important stage in the development of wear resistant materials, which provide increased durability of friction components operating under specified conditions.

Russian scientists were the first to demonstrate that one of the main polymer wear mechanisms is the fatigue failure of the surface layers of friction materials [1–6]. The fatigue nature of wear was also confirmed by other researchers [7, 8]. Although the fatigue type of wear is the least intense, it is the main one for particular friction units. Kragelsky and Nepomnyashchy [5] studied the sliding of a spherical indenter on a rubber disk. They found that initially the sliding ball leaves a barely visible friction trace on the disk, then the indenter slides for a long time without significant changes, and finally the most intensive entrainment of debris from the path begins after a certain number of cycles. Thus, the stage of damage accumulation (so-called incubation period) and the stage of intensive wear were distinguished. The authors revealed a correlation between the results of frictional contact fatigue tests and conventional bulk fatigue tests under cyclic loading (curves of the number of cycles to failure versus the applied load were parallel). Eiss [9] investigated fatigue wear during sliding of a metal ball on specimens made of various polymers (polycarbonate, polyvinyl chloride, ultra-high molecular weight polyethylene, etc.). His investigation results showed that the number of cycles to the onset of wear is inversely proportional to the ratio between tensile stress in the contact area and tensile yield strength. The rate of wear after the incubation period was found to be proportional to the modulus of elasticity.

Strains are most often taken as criteria of defect nucleation in the experimental investigation of the fatigue

process under uniaxial loading and torsion, because they can easily be determined experimentally through displacements [10]. The most used strains are the maximum principal strains [11–13], and the less used are the octahedral shear strains [10]. The results of conventional fatigue tests, especially those obtained under multiaxial loading, can be applied in fatigue wear modeling [14–16]. The theory of strength of materials considered the reduced stress as one of the criteria for the occurrence of a highly elastic state [17]. The reduced stress was used in the fatigue failure criterion in the experiments of Kragelsky and Nepomnyashchy [5] based on Saverin's solution of a contact problem [18].

The main reason for the fatigue failure of the material surface layers is the surface roughness of the contacting bodies, which causes a cyclic variation of the stress field in the surface layers of the material.

Approaches to the modeling of fatigue wear of elastic materials are overviewed in Ref. [19]. Our earlier papers discussed wear models based on the maximum shear stress criterion for an elastic half-space [20, 21] and for coated materials [22]. We also proposed a wear model based on considering a thermokinetic model of damage accumulation in the surface layers of the contacting bodies in sliding friction [23].

This paper reports the modeling results on fatigue wear of elastomers obtained with the use of the reduced stress criterion, which was confirmed experimentally in Ref. [5].

2. THE MAIN STAGES OF FATIGUE WEAR MODELING OF ELASTOMERS

According to Ref. [19], the main stages of fatigue wear modeling are:

– solution of a contact problem between sliding deformable bodies with rough surfaces, and determination of stresses in the surface layers of materials;

– selection of a damage accumulation criterion that is usually related to the stress amplitude values, calculation of the damage function at different points in time;

– modeling of fatigue crack initiation and growth after the critical damage value is reached, and modeling of wear debris separation;

– determination of the shape of the formed surface, and calculation of the damage function for the rest of the material, taking into account the stresses at the contact of surfaces with changed microgeometry and the damage present in the contacting bodies with changed microgeometry;

– calculation of linear or mass wear as a function of time or distance covered.

This paper considers a simplified model of contact interaction: the sliding of a system of spherical asperities (rough surface model of a rigid counterbody) over a viscoelastic half-space (elastomer model). The model, on the one hand, reflects the main contact interaction features of rough bodies associated with the cyclic deformation of the surface layers of the contacting bodies and leading to fatigue damage formation in the subsurface layers of the material and wear. On the other hand, it describes the effect of the main process parameters (mechanical and strength properties of contacting bodies, surface microgeometry, load, sliding velocity) on the rate of material wear by the fatigue mechanism.

2.1. Solution of a Sliding Contact Problem for a System of Asperities on a Viscoelastic Half-Space

Let us consider the sliding of a system of n identical punches (asperities) over a viscoelastic half-space with constant velocity V (Fig. 1). The surface shape of the asperities is described by the functions $f_i(x, y)$ obtained by transforming the function $f(x,y) = (x^2 + y^2)/(2r)$ (r is the asperity radius) by shifting along the Ox axis. The

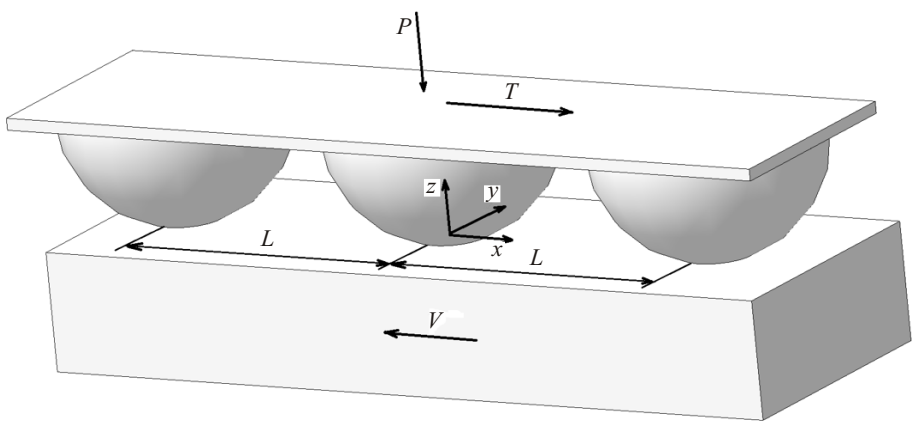

Fig. 1. Scheme of contact.

system is subjected to vertical force P and horizontal force T to provide a constant sliding velocity. The mutual spatial arrangement of the asperities is unchanged. For definiteness, we consider a configuration in which the symmetry axes of the asperities are in the same plane at a distance L from each other. The Cartesian coordinate system is associated with the system of moving asperities, and its center is at the point of intersection between the axis of a fixed asperity and the undeformed surface of the half-space.

The following conditions hold at the half-space boundary:

$$z = 0:\ \tau_{xz}(x, y) = 0,\ \tau_{yz}(x, y) = 0,$$

$$\sum_{q=1}^{n} w_{iq}(x, y) = f_i(x, y) - D\ ,\ (x, y) \in \Omega_i,\ \ i = 1, ..., n,$$
$$\sigma_z(x, y) = 0,\ \tau_{xz}(x, y) = 0,\ \tau_{yz}(x, y) = 0,\ (x, y) \notin \Omega_i, \quad (1)$$
$$-\infty < x < +\infty,\ -\infty < y < +\infty,$$

where Ω_i $(i = 1, ..., n)$ are the contact areas of the asperities, $w_{iq}(x, y)$ $(i, q = 1, ..., n)$ is the vertical displacement of the half-space boundary inside a fixed ith region Ω_i due to pressure inside the contact areas, D is the distance between the contact surfaces, and σ_z, τ_{xz}, τ_{yz} are the normal and tangential stresses. Tangential stresses are assumed to be absent in the contact area.

The equilibrium equation reads:

$$P = \sum_{i=1}^{n} \iint_{\Omega_i} p_i(x, y)\mathrm{d}x\mathrm{d}y, \quad (2)$$

where $p_i(x, y)$ is the contact pressure on the contact area between the ith asperity and the half-space.

The mechanical properties of the viscoelastic half-space are described by the following relations between stresses and strains given by the Volterra integral operator:

$$\gamma_{xy}(t) = \frac{1}{G}\tau_{xy}(t) + \frac{1}{G}\int_{-\infty}^{t} \tau_{xy}(\tau)K(t-\tau)\mathrm{d}\tau,$$

$$\gamma_{yz}(t) = \frac{1}{G}\tau_{yz}(t) + \frac{1}{G}\int_{-\infty}^{t} \tau_{yz}(\tau)K(t-\tau)\mathrm{d}\tau,$$

$$\gamma_{zx}(t) = \frac{1}{G}\tau_{zx}(t) + \frac{1}{G}\int_{-\infty}^{t} \tau_{zx}(\tau)K(t-\tau)\mathrm{d}\tau,$$

$$e_x(t) = \frac{1}{E}\Big[\sigma_x(t) - \nu(\sigma_y(t) + \sigma_z(t))\Big] \quad (3)$$

$$+\frac{1}{E}\int_{-\infty}^{t} \Big[\sigma_x(\tau) - \nu(\sigma_y(\tau) + \sigma_z(\tau))\Big]K(t-\tau)\mathrm{d}\tau,$$

$$e_y(t) = \frac{1}{E}\Big[\sigma_y(t) - \nu(\sigma_x(t) + \sigma_z(t))\Big]$$

$$+\frac{1}{E}\int_{-\infty}^{t} \Big[\sigma_y(\tau) - \nu(\sigma_x(\tau) + \sigma_z(\tau))\Big]K(t-\tau)\mathrm{d}\tau,$$

$$e_z(t) = \frac{1}{E}\Big[\sigma_z(t) - \nu(\sigma_y(t) + \sigma_x(t))\Big]$$

$$+\frac{1}{E}\int_{-\infty}^{t} \Big[\sigma_z(\tau) - \nu(\sigma_y(\tau) + \sigma_x(\tau))\Big]K(t-\tau)\mathrm{d}\tau,$$

$$K(t') = \sum_{i=1}^{s} k_i \exp\left(-\frac{t'}{\lambda_i}\right),$$

where ν is the Poisson's ratio, e_x, e_y, e_z, γ_{xy}, γ_{yz}, γ_{zx} are the strain tensor components, E and G are the Young's modulus and shear modulus, respectively. The creep kernel $K(t)$ is a combination of exponential functions with the relaxation spectrum $1/k_i$ and retardation spectrum λ_i.

The problem is solved using the boundary element method described elsewhere for the case of one indenter [24, 25] and two indenters [26]. The method was modified in this study to reduce the computational time by taking into account the short- and long-range effects for the asperities spaced at a large distance.

For each asperity, we choose a rectangular region Ω_i^0, $i = 1, ..., n$ of size $a_i \times b_i$ that contains a contact area. Meshes of size $Na_i \times Nb_i = N_i$, $i = 1, ..., n$ are generated inside the regions, with a constant pressure p_j^i, $i = 1, ..., n$, $j = 1, ..., N_i$ inside each element. The vertical displacement of the half-space boundary at a point is a superposition of displacements at this point caused by the pressure in each mesh element. Let us consider the column $\| w^{iq} \|$ of vertical boundary displacements inside the region Ω_i^0 due to the pressure $\| p^q \|$ inside the region Ω_q^0. The dependence of the vertical displacements on the contact pressure can be expressed using the matrix $\| A^{iq} \|$ of $N_i \times N_q$ elements:

$$\| A^{iq} \| \cdot \| p^q \| = \| p^q \|. \quad (4)$$

The matrix coefficients A_{jl}^{iq}, $j = 1, ..., N_i$, $l = 1, ..., N_q$, are the vertical displacement at the center of the element j of the region Ω_i^0 caused by the unit pressure in the element l of the region Ω_q^0. They can be calculated using the expression derived in Ref. [24]:

$$w(x', y') = -\frac{2}{\pi^2 c}$$

$$\times \iint_{\Omega^*} \left\{ \frac{1}{\sqrt{(x'-\xi')^2 + (\eta'-y')^2}} \right\} \mathrm{d}\xi'\mathrm{d}\eta'$$

$$-\frac{2}{\pi^2 c} \iint_{\Omega^*} \sum_{j=1}^{s} \left\{ B_j e^{A_j(x'-\xi')} \right.$$

$$\left. \times \int_{A_j(x'-\xi')}^{\infty} \frac{e^{-u}\mathrm{d}u}{\sqrt{u^2 + A_j^2(\eta'-y')^2}} \right\} \mathrm{d}\xi'\mathrm{d}\eta',$$

$$(x', y', \xi', \eta') = \frac{(x, y, \xi, \eta)}{r}, \quad A_j = \frac{r}{\lambda_j V},$$

$$B_j = k_j \cdot \frac{r}{V}, \quad k_j = \frac{c}{\lambda_j}, \quad j = 1, ..., s, \tag{5}$$

$$P' = \frac{P}{G_l r^2}, \; p'(x, y) = \frac{p(x, y)}{G_l}.$$

The parameter c relates the relaxation and retardation times. Using boundary conditions (1) and equilibrium condition (2), we come to the following system of linear equations:

$$\begin{bmatrix} \begin{pmatrix} A_{11}^{11} & \cdots & A_{N_1 1}^{11} \\ \vdots & \ddots & \vdots \\ A_{1N_1}^{11} & \cdots & A_{N_1 N_1}^{11} \end{pmatrix} & \cdots & \begin{pmatrix} A_{11}^{1n} & \cdots & A_{N_n 1}^{1n} \\ \vdots & \ddots & \vdots \\ A_{1N_1}^{1n} & \cdots & A_{N_n N_1}^{1n} \end{pmatrix} & 1 \\ \vdots & \ddots & \vdots & \vdots \\ \begin{pmatrix} A_{11}^{1n} & \cdots & A_{N_1 1}^{1n} \\ \vdots & \ddots & \vdots \\ A_{1N_n}^{1n} & \cdots & A_{N_1 N_n}^{1n} \end{pmatrix} & \cdots & \begin{pmatrix} A_{11}^{nn} & \cdots & A_{N_n 1}^{nn} \\ \vdots & \ddots & \vdots \\ A_{1N_n}^{nn} & \cdots & A_{N_n N_n}^{nn} \end{pmatrix} & 1 \\ (s^1 \; \cdots \; s^1) & \cdots & (s^n \; \cdots \; s^n) & 0 \end{bmatrix}$$

$$\times \begin{bmatrix} \begin{pmatrix} p_1^1 \\ \vdots \\ p_{N_1}^1 \end{pmatrix} \\ \vdots \\ \begin{pmatrix} p_1^n \\ \vdots \\ p_{N_n}^n \end{pmatrix} \\ D' \end{bmatrix} = \begin{bmatrix} \begin{pmatrix} f_1^1 \\ \vdots \\ f_{N_1}^1 \end{pmatrix} \\ \vdots \\ \begin{pmatrix} f_1^n \\ \vdots \\ f_{N_n}^n \end{pmatrix} \\ P' \end{bmatrix}. \tag{6}$$

Here, s^i, $i = 1, ..., n$ are the element grid areas in the corresponding regions Ω_i^0, p_j^i is the pressure inside the jth element grid of the region Ω_i^0, and f_j^i is the value of the function $f_i(x, y)$, $i = 1, ..., n$ at the center of the jth element grid of the region Ω_i^0. After the iteration procedure, which included the solution of the system and the subsequent reduction of the rank of its augmented matrix by zeroing elements with negative pressure, we determined the unknown contact areas, pressure distribution, and the depth of system penetration $D' = D/r$.

2.2. Calculation of Stresses with Taking into Account the Interaction of Asperities

The considered boundary conditions (1) imply the absence of tangential stresses in the contact area, so we can use the solution of the Boussinesq problem [27] to calculate stresses in the half-space. By summing over all loaded surface elements, we can determine the stress components at any point inside the half-space:

$$\sigma_x(x', y', z') = \frac{1}{2\pi}\sum_{i=1}^{n}\Bigg(p_i' \iint\limits_{\Omega_i'} \frac{1-2\nu}{(r^*)^2} \times \Bigg(\left(1 - \frac{z'}{\rho}\right)\frac{(x'-\xi')^2 - (y'-\zeta')^2}{(r^*)^2} + \frac{z'(y'-\zeta')^2}{\rho^3} \Bigg) d\xi' d\zeta' - p_i' \iint\limits_{\Omega_i'} \frac{3z'(x'-\xi')^2}{\rho^5} d\xi' d\zeta' \Bigg),$$

$$\sigma_y(x', y', z') = \frac{1}{2\pi}\sum_{i=1}^{n}\Bigg(p_i' \iint\limits_{\Omega_i'} \frac{1-2\nu}{(r^*)^2} \times \Bigg(\left(1 - \frac{z'}{\rho}\right)\frac{(y'-\zeta')^2 - (x'-\xi')^2}{(r^*)^2} + \frac{z'(x'-\xi')^2}{\rho^3} \Bigg) d\xi' d\zeta' - p_i' \iint\limits_{\Omega_i'} \frac{3z'(y'-\zeta')^2}{\rho^5} d\xi' d\zeta' \Bigg),$$

$$\sigma_z(x', y', z') = -\frac{3}{2\pi}\sum_{i=1}^{n} p_i' \iint\limits_{\Omega_i'} \frac{z'^3}{\rho^5} d\xi' d\zeta', \tag{7}$$

$$\tau_{xy}(x', y', z') = \frac{1}{2\pi}\sum_{i=1}^{n}\Bigg(p_i' \iint\limits_{\Omega_i'} \frac{1-2\nu}{(r^*)^2} \times \Bigg(\left(1 - \frac{z'}{\rho}\right)\frac{(x'-\xi')(y'-\zeta')}{(r^*)^2} - \frac{z'(y'-\zeta')(x'-\xi')}{\rho^3} \Bigg) d\xi' d\zeta' - p_i' \iint\limits_{\Omega_i'} \frac{3z'(x'-\xi')(y'-\zeta')}{\rho^5} d\xi' d\zeta' \Bigg),$$

$$\tau_{xz}(x', y', z') = -\frac{3}{2\pi}\sum_{i=1}^{n} p_i' \iint\limits_{\Omega_i'} \frac{(x'-\xi')z'^2}{\rho^5} d\xi' d\zeta',$$

$$\tau_{yz}(x', y', z') = -\frac{3}{2\pi}\sum_{i=1}^{n} p_i' \iint\limits_{\Omega_i'} \frac{(y'-\zeta')z'^2}{\rho^5} d\xi' d\zeta',$$

$$\rho^2 = (x'-\xi')^2 + (y'-\zeta')^2 + z'^2,$$

$$(r^*)^2 = (x'-\xi')^2 + (y'-\zeta')^2.$$

2.3. Calculation of Damage Accumulation and Contact Fatigue Wear

Damage accumulation, which is characterized by the function $Q(x, y, z, t)$ nondecreasing in time, can be studied using a linear damage summation model (the damage

increment at each time point does not depend on the amount of accumulated damage) [19]. Failure occurs at the time point t^*, when this function reaches a predetermined threshold value.

The damage accumulation rate depends on the material properties and contact interaction conditions. The choice of a damage accumulation model is usually based on experimental data. For elastomers, the results obtained in Ref. [5] are classical and can be used to construct a model of damage accumulation in the surface layers of elastomers. In this paper, the number of cycles to failure is associated with the values of reduced stresses. In accordance with the hypothesis of linear damage summation, we write the following relation for the damage accumulation rate [19]:

$$q(x, y, z, t) = \frac{\partial Q(x, y, z, t)}{\partial t} = g\left(\frac{\Delta\sigma_p(x, y, z, t)}{E}\right)^m, \quad (8)$$

where g and m are experimentally determined constants, and $\Delta\sigma_p(x, y, z, t)$ are the amplitude values of reduced stresses at the point (x, y, z). To calculate the reduced stresses [17], we first determine the stress tensor components based on Eq. (7) and then determine the principal stresses $\sigma_1, \sigma_2, \sigma_3$ $(\sigma_1 > \sigma_2 > \sigma_3)$ as the roots of the equation:

$$\det\begin{vmatrix} \sigma_x - \sigma & \tau_{xy} & \tau_{xz} \\ \tau_{yx} & \sigma_y - \sigma & \tau_{yz} \\ \tau_{zx} & \tau_{zy} & \sigma_z - \sigma \end{vmatrix} = 0. \quad (9)$$

Then the reduced stress is defined by the formula

$$\sigma_p = \frac{1}{\sqrt{2}}\sqrt{(\sigma_1 - \sigma_2)^2 + (\sigma_2 - \sigma_3)^2 + (\sigma_3 - \sigma_1)^2}. \quad (10)$$

In sliding of the considered system of punches, the damage function is independent of the x and y coordinates and is a function of only the z coordinate and time t, which can be expressed in terms of the number of cycles N, i.e., $Q = Q(z, N)$.

By calculating the stress distribution in the viscoelastic half-space, we determine the maximum values of reduced stresses along the Ox axis, which coincides with the sliding direction of the system of indenters. The maximum amplitudes of reduced stresses referred to Young's modulus E will be denoted as $\tilde{\sigma}_p(z)$. They are attained in the plane passing through the geometric center of the contact area.

Based on Eq. (8), we can calculate the damage $Q(z, N)$ accumulated at an arbitrary fixed point z for N cycles using the relation

$$Q(z, N) = \int_0^N q_n(z, n)\Delta t\,dn + Q_0(z), \quad (11)$$

where $Q_0(z)$ is the initial damage distribution in the material, Δt is the time of one cycle, and $q_n(z, n)$ is the damage accumulation rate independent of the x and y coordinates.

Failure will occur when damage at some point reaches a critical value. In a normalized reference frame, this condition can be written as

$$Q(z, N^*) = 1, \quad (12)$$

where N^* is the number of cycles to failure.

Equations (8), (11), and (12) yield a relation for calculating the number of cycles to failure under an alternating stress field:

$$\int_0^{N^*} g(\tilde{\sigma}_p(z))^m \Delta t\,dn + Q_0(z) = 1. \quad (13)$$

At zero initial damage, the number of cycles to the first failure occurring at depth h, where the reduced stresses reach a maximum, can be determined using the relation that follows from Eq. (13):

$$N^* = (g\Delta t(\max\tilde{\sigma}_p(z))^m)^{-1}, \quad Q^*(z) = N^* g\Delta t(\tilde{\sigma}_p(z))^m, \ z \le -h. \quad (14)$$

Here, $Q^*(z)$ is the damage that should be further taken into account in the study of the accumulation process.

Since after delamination and removal of the material the value of the function $Q^*(z)$ on the newly formed surface is very close to critical, surface wear necessarily occurs after the first failure event. It should be noted that the function $\tilde{\sigma}_p(z)$ can have a maximum on the surface and hence the value of h is determined only by the calculation mesh size.

As was shown earlier [19, 20], surface wear can also be accompanied by subsurface failure, i.e., a discrete change in the layer thickness; the probability of such a scenario is determined mainly by the value of the parameter m. So, at $m = 2$ (and at lower parameter values), after the first subsurface failure event there occurs only surface wear.

Analysis of the results obtained in Ref. [5] suggests that the experimental findings can be described by Eq. (8), and the parameter m for the elastomers considered in Ref. [5] is almost the same and close to 0.3, while the parameter g is significantly different.

3. ANALYSIS OF CALCULATION RESULTS

Analysis of stresses, contact fatigue damage accumulation, and wear kinetics was carried out using the fol-

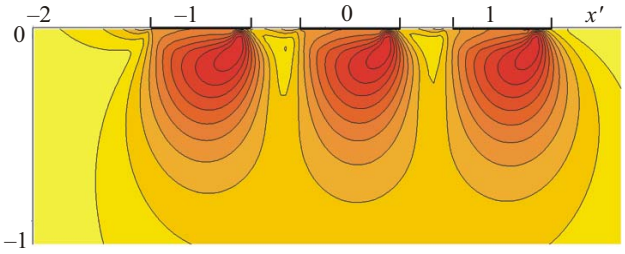

Fig. 2. Distribution of reduced stresses in the *XZ* plane. $\lambda_{1,2,3}$ = 0.001, 0.005, 0.0002, c = 5, ν = 0.47, P' = 0.12, L' = 1.0, V' = 1.25 (color online).

lowing dimensionless parameters for three retardation times:

$$(x', y', z', \xi', \eta') = (x, y, z, \xi, \eta)/r,$$
$$L' = \frac{L}{r},\ A_j = \frac{r}{\lambda_j V},\ B_j = k_j \frac{r}{V},$$
$$c, \lambda_j,\ P' = \frac{P}{G_l r^2},\ p'(x, y) = \frac{p(x, y)}{G_l}, \quad (15)$$
$$V' = (V/r)\cdot 1\ \text{s},\ j = 1, 2, 3.$$

The stresses arising in the case of a single indenter sliding along the boundary of a viscoelastic half-space were analyzed elsewhere [28, 29]. Particularly, it was shown that the maximum tensile stresses occur on the surface, which can lead to surface cracking if the threshold values determined by the strength properties of the material are exceeded. In this study, the function of contact fatigue damage accumulation is associated with reduced stresses, so we will analyze only the function $\tilde{\sigma}_p$ here.

The distribution of reduced stresses under the half-space surface in the *XZ* plane is demonstrated in Fig. 2. The contact area boundaries of three asperities are shown on the surface. The stress distribution is asymmetric relative to the center of the contact areas because the material is viscoelastic. The points of maximum reduced stresses are located at a distance from the half-space surface under the asperity contact areas. Figure 3 illustrates the dependence of the maximum reduced stresses on the z' coordinate for different sliding velocities. The maximum stress values increase with increasing sliding velocity.

The effect of the parameter c, which characterizes the viscoelastic properties of the half-space material, on the distribution of maximum reduced stresses is shown in Fig. 4. For comparison, the figure illustrates the results obtained for an elastic material (curve *1*). As c increases, the values of reduced stresses increase and the maximum point shifts closer to the half-space surface.

The fatigue wear kinetics was analyzed by calculating the contact fatigue damage accumulation. The linear dependence of damage on the parameter g in Eq. (8) allows it to be included in the dimensionless group $S' = gN\Delta tL'$, which characterizes the friction path. The value of m, as noted in the previous section, can be taken equal to 0.3 for some rubbers and used in the calculations.

Figure 5 displays the calculation results on the kinetics of contact fatigue wear at different sliding velocities. A common feature caused by the concentration of reduced stresses under the surface is the presence of an incubation period, observed experimentally [5]. The higher is the sliding velocity of asperities, the shorter is the friction path to the first failure event followed by the separation of a finite thickness layer. The lower is the velocity, the larger is the thickness of the detached layer at the beginning of the wear process. Then comes the stage of continuous surface wear, and the wear rate in the early

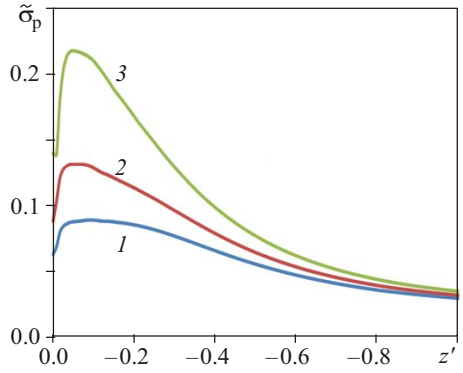

Fig. 3. In-depth distribution of maximum reduced stresses. $\lambda_{1,2,3}$ = 0.001, 0.005, 0.0002, c = 5, ν = 0.47, P' = 0.12, L' = 1.0, V' = 0.5 (*1*), 1.25 (*2*), 3.5 (*3*) (color online).

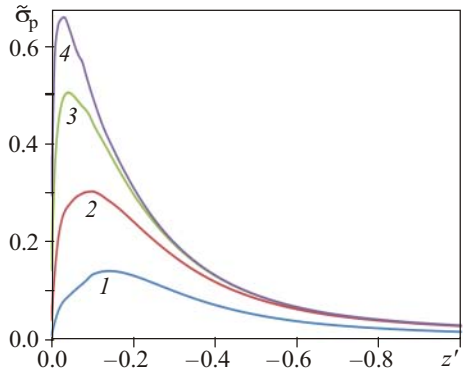

Fig. 4. In-depth distribution of maximum reduced stresses. $\lambda_{1,2,3}$ = 0.001, 0.005, 0.0002, V' = 3.0, ν = 0.47, P' = 0.12, L' = 1.0, c = 5 (*2*), 20 (*3*), 50 (*4*), curve *1* corresponds to the elastic half-space (color online).

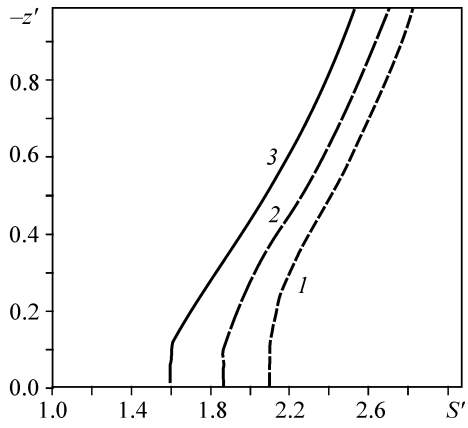

Fig. 5. Surface displacement due to wear depending on the friction path at different sliding velocities: $V' = 0.5$ (*1*), 1.25 (*2*), 3.0 (*3*), $c = 5$, $\nu = 0.47$, $P' = 0.12$, $L' = 1.0$, $\lambda_{1,2,3} = 0.001$, 0.005, 0.0002.

stage is higher in the case of a longer incubation period. At a later stage, the dependence of the surface displacement on the friction path tends to be linear, which means the tendency to a steady-state wear rate; the value of this steady-state wear rate for the considered set of parameters weakly depends on the sliding speed.

The viscoelastic properties of the material are essentially characterized by the value of the parameter c. For an elastic material, $c = 1$. We calculated the wear kinetics for different values of c at two fixed sliding velocities (Fig. 6). It should be noted that the longer is the incubation period, the larger is the thickness of the layer detached after the completion of this period. In the case of an elastic material (compared to a viscoelastic), the incubation period is longer and the steady-state wear rate is lower. At higher sliding velocities, the effect of the rheological properties of the material is more pronounced, which has an impact on the duration of the incubation period and the detached layer thickness. Interestingly, the transition from an elastic to viscoelastic material, for which $c = 5$, is characterized by significant changes in the wear kinetics, especially at the run-in stage, while a further increase in c to 50 has a smaller effect.

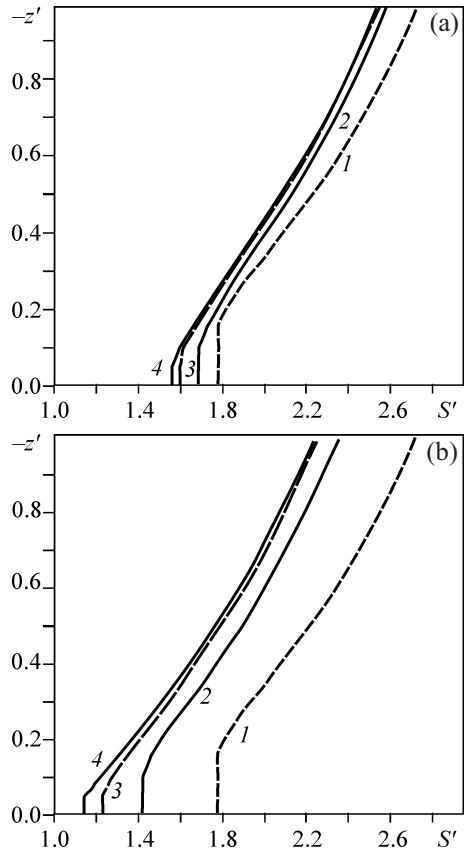

Fig. 6. Surface displacement due to wear depending on the friction path for different viscoelastic properties of the material for two sliding velocities: $V' = 3$ (a) and 10 (b), $c = 1$ (*1*), 5 (*2*), 20 (*3*), 50 (*4*), $\nu = 0.47$, $\lambda_{1,2,3} = 0.001$, 0.005, 0.0002, $P' = 0.12$, $L' = 1.0$.

4. CONCLUSIONS

A method has been developed for the calculation of contact fatigue damage in the surface layers of elastomers in sliding friction conditions, including:

– solution of a sliding contact problem for a system of spherical asperities on the surface of a viscoelastic half-space,

– analysis of stresses in the surface layers,

– calculation of the damage function in accordance with the chosen damage accumulation criterion.

A model calculation of contact fatigue damage accumulation under the assumption of the validity of the linear damage summation hypothesis showed that the friction path, which implies the incubation period, depends on the sliding velocity and viscoelastic properties of the material. By analyzing the dependence of the wear rate on the input parameters of the problem, we established the effect of the sliding velocity on the time of fatigue damage initiation and the wear rate at the run-in and steady-state wear stages for materials with different rheological properties. It was found that the surface wear rate after the incubation period increases smoothly and then stabilizes. The presence of the steady-state wear rate agrees well with experimental data [5].

The proposed method for studying contact fatigue in viscoelastic materials can also be applied on the macroscale to determine the possible crack initiation site. Mechanisms of further crack propagation can be studied using Barenblatt's methods [30].

FUNDING

The work was carried out as part of a government assignment (State Reg. No. AAAA-A17-117021310379-5). The analysis of wear of rubber materials was partially supported by Russian Foundation for Basic Research (project No. 19-08-00615).

REFERENCES

1. Ratner, S.B., Wear of Polymers as a Fatigue Fracture Process, in *Theory of Friction and Wear*, Ratner, S.B., Klitenik, G.S., and Lurie, E.G., Eds., Moscow: Nauka, 1965, pp. 156–159.
2. Ratner, S.B. and Lurie, E.G., Abrasion of Polymers as a Thermally Activated Kinetic Process, *Dokl. AN SSSR*, 1966, vol. 166, no. 4, pp. 909–912.
3. *Frictional Wear of Rubber: Coll. Papers*, Evstratov, V.F., Ed., Moscow: Knimia, 1964.
4. Kragelsky, I.V. and Nepomnyashchy, E.F., Fatigue Mechanism in Elastic Contact, in *Mechanics and Mechanical Engineering*, Moscow: Izd-vo AN SSSR, 1963, pp. 49–56.
5. Kragelsky, I.V. and Nepomnyashchy, E.F., Theory of Wear of Highly Elastic Materials, in *Plastics in Sliding Bearings*, Moscow: Nauka, 1965, pp. 49–56.
6. Kragelsky, I.V., Reznikovsky, M.M., Brodsky, G.I., and Nepomnyashchy, E.F., Friction Contact Fatigue of Highly Elastic Materials, *Kauchuk Rezina*, 1965, no. 9, pp. 30–34.
7. Clark, W.T. and Lancaster, J.K., Breakdown and Surface of Carbons during Repeated Sliding, *Wear*, 1963, vol. 6, no. 6, pp. 467–482.
8. Kerridge, M. and Lancaster, J.K., The Stages in a Process of Severe Metallic Wear, *Proc. Roy. Soc.*, 1956, vol. 236, pp. 250–254.
9. Eiss, N.S., Jr., Fatigue Wear of Polymers, *ACS Symposium Series*, 1984, vol. 50, pp. 78–82.
10. Mars, W.V. and Fatemi, A., A Literature Survey of Fatigue Analysis Approaches for Rubber, *Int. J. Fatigue*, 2002, vol. 24, pp. 949–961.
11. Cadwell, S.M., Merrill, R.A., Sloman, C.M., and Yost, F.L., Dynamic Fatigue Life of Rubber, *Ind. Eng. Chem.*, 1940, vol. 12, pp. 19–23.
12. Fielding, J.H., Flex Life and Crystallization of Synthetic Rubber, *Ind. Eng. Chem.*, 1943, vol. 35, no. 12, pp. 1259–1261.
13. *Handbook of Molded and Extruded Rubber*, Goodyear Tire and Rubber Company, 1969.
14. Ayoub, G., Naït-Abdelaziz, M., and Zaïri, F., Multiaxial Fatigue Life Predictors for Rubbers: Application of Recent Developments to a Carbon-Filled SBR, *Int. J. Fatigue*, 2014, vol. 66, pp. 168–176.
15. Jardin, A., Leblond, J.-B., Berghezan, D., and Portigliatti, M., Theoretical Modelling and Experimental Study of the Fatigue of Elastomers under Cyclic Loadings of Variable Amplitude, *Comp. Rend. Mécan.*, 2014, vol. 342, no. 8, pp. 450–458.
16. Zhang, J., Xue, F., Wang, Y., Zhang, X., and Han, S., Strain Energy-Based Rubber Fatigue Life Prediction under the Influence of Temperature, *R. Soc. Open Sci.*, 2018, vol. 5, p. 180951.
17. Bezukhov, N.I., *Fundamentals of the Theory of Elasticity, Plasticity, and Creep*, Moscow: Vysshaya Shkola, 1961.
18. Kostetsky, B.I., Friction and Wear in Machine Parts, in *Proc. 2nd All-Union Conf. on Friction and Wear in Machines, Vol. 4*, Moscow: USSR Academy of Sciences, 1951, pp. 201–208.
19. Goryacheva, I.G., *Mechanics of Frictional Interaction*, Moscow: Nauka, 2001.
20. Goryacheva, I.G. and Chekina, O.G., Model of Fatigue Fracture of Surfaces, *Sov. J. Frict. Wear*, 1990, vol. 11, no. 3, pp. 389–400.
21. Goryacheva, I.G. and Chekina, O.G., Surface Wear: From Microfracture Modeling to Shape Change Analysis, *Izv. RAN. MTT*, 1999, no. 5, pp. 131–147.
22. Goryacheva, I.G. and Torskaya, E.V., Modeling of Fatigue Wear of a Two-Layered Elastic Half-Space in Contact with Periodic System of Indenters, *Wear*, 2010, vol. 268, no. 11–12, pp. 1417–1422.
23. Chekina, O.G., Modeling of Fracture of Surface Layers in Contact of Rough Bodies, *Prochn. Plastich.*, 1996, vol. 1, pp. 186–191.
24. Aleksandrov, V.M., Goryacheva, I.G., and Torskaya, E.V., Sliding Contact of a Smooth Indenter and a Viscoelastic Half-Space (3D Problem), *Dokl. Phys.*, 2010, vol. 55, no. 2, pp. 77–80.
25. Goryacheva, I.G., Stepanov, F.I., and Torskaya, E.V., Sliding of a Smooth Indentor over a Viscoelastic Half-Space When There is Friction, *J. Appl. Math. Mech.*, 2015, vol. 79, no. 6, pp. 596–603.
26. Stepanov, F.I., Sliding of Two Smooth Indenters on a Viscoelastic Foundation in the Presence of Friction, *J. Appl. Mech. Tech. Phys.*, 2015, vol. 56, no. 6, pp. 1071–1077.
27. Johnson, K.L., *Contact Mechanics*, Cambridge: Cambridge University Press, 1985.
28. Stepanov, F.I. and Torskaya, E.V., Study of Stress State of Viscoelastic Half-Space in Sliding Contact with Smooth Indenter, *J. Frict. Wear*, 2016, vol. 37, no. 2, pp 101–106.
29. Goryacheva, I.G., Makhovskaya, Yu.Yu., Morozov, A.V., and Stepanov, F.I., *Friction of Elastomers: Modeling and Experiment*, Moscow: Izhevsk Institute of Computer Science, 2017.
30. Barenblatt, G.I., *Flow, Deformation and Fracture: Lectures on Fluid Mechanics and the Mechanics of Deformable Solids for Mathematicians and Physicists*, Cambridge: Cambridge University Press, 2014.